Iranian Journal of Basic Medical Sciences

ijbms.mums.ac.ir

Comparative analysis of second and third-generation nanobody-based CAR-NK cells targeting PSMA in prostate cancer immunotherapy: *In silico* and *in vitro* studies

Masoud Gandomkar Ghalhar [1], Arezoo Karami Vandishi [2], Akram Ramazani [1], Fatemeh Hajari Taheri [3], Zahra Sharifzadeh [4], Mohsen Abolhassani [4], Masoud Soleimani [2], Niloofar Taghipour [2], Wytske M van Weerden [5], Mojgan Bandehpour [6], Mahmoud Hassani [7, 8]*, Kowsar Bagherzadeh [9]*

[1] Department of Medical Biotechnology, School of Advanced Technologies in Medicine, Shahid Beheshti University of Medical Sciences, Tehran, Iran
[2] Department of Tissue Engineering and Applied Cell Science, School of Advanced Technologies in Medicine, Shahid Beheshti University of Medical Sciences, Tehran, Iran
[3] Food and Drug Laboratory Research Center (FDLRC), Iran Food and Drug Administration (IFDA), MOH & M[illegible] Tehran, Iran
[4] Hybridoma Lab, Department of Immunology, Pasteur Institute of Iran, Tehran, Iran
[5] Department of Urology, Erasmus Medical Center, Rotterdam, The Netherlands
[6] Cellular and Molecular Biology Research Center, Shahid Beheshti University of Medical Sciences, Tehran, Iran
[7] Medical Nanotechnology and Tissue Engineering Research Center, Shahid Beheshti University of Medical Sciences, Tehran, Iran
[8] Department of Molecular Medicine, School of Advanced Technologies in Medicine, Shahid Beheshti University of Medical Sciences, Tehran, Iran
[9] Eye Research Center, Five Senses Health Institute, Rassoul Akram Hospital, Iran University of Medical Sciences, Tehran, Iran

ARTICLE INFO

Article type:
Original

Article history:
Received: Oct 21, 2025
Accepted: May 18, 2026

Keywords:
Chimeric antigen receptor
Natural killer cell
Single-domain antibodies (Nanobodies)
Prostate-specific membrane antigen (PSMA)
Prostatic neoplasms
OX40 co-stimulatory domain
Molecular dynamics - simulation

ABSTRACT

Objective(s): The use of CAR technology in the treatment of cancer cells is progressing, as well as the use of CAR T-cell in the treatment of blood malignancies is in the clinical trial stage. In this study, have compared the second and third generation CAR expressed in NK cells in dealing with prostate cancer cells.

Materials and Methods: To optimize the CAR design for detection of NK-92 cells, an *in silico* approach to select between two tags (Flag and c-Myc tags) was initially employed, ultimately favoring the Flag tag. By using lentiviral particles, transduced NK-92 cells with second- and third-generation CAR constructs were subsequently tested as effector cells against prostate cancer cells expressing the Prostate-Specific Membrane Antigen (PSMA). Then assessed both cytokine secretion and cytotoxic responses.

Results: Computational analysis indicated that the NB/Flag/hinge configuration would provide superior PSMA recognition. Flow cytometry confirmed successful CAR expression in 47% of second-generation and 49% of third-generation NK-92 cells. Upon co-culture with PSMA-positive LNCaP cells and PSMA-negative PC-3 cells, the third-generation CAR NK cells demonstrated a noticeably stronger cytotoxic effect. Furthermore, higher levels of IL-2, TNF-α, and IFN-γ secretion were observed in the third-generation CAR group compared to the second.

Conclusion: According to the computational studies, NB/Flag/hinge interacts with PSMA primarily through electrostatic forces. More importantly, third-generation CAR NK cells targeting PSMA displayed enhanced cytotoxicity and cytokine production relative to second-generation counterparts, pointing to their greater potential for therapeutic application.

▶ Please cite this article as:
Gandomkar Ghalhar M, Karami Vandishi A, Ramazani A, Hajari Taheri F, Sharifzadeh Z, Abolhassani M, Soleimani M, Taghipour N, van Weerden WM, Bandehpour M, Hassani M, Bagherzadeh K. Comparative analysis of second and third-generation nanobody-based CAR-NK cells targeting PSMA in Prostate cancer immunotherapy: *In silico* and *in vitro* studies. Iran J Basic Med Sci 2026; 29:

Introduction

Despite significant advances in the diagnosis and treatment of prostate cancer, it remains the second most common cancer and the third leading cause of cancer-related mortality among men (1, 2). In recent years, advancements in cancer immunotherapy have been particularly remarkable. The clinical application of T cells engineered with chimeric antigen receptors (CAR) in the treatment of hematologic malignancies has garnered considerable attention (3). CAR-T cell-based immunotherapy has achieved significant progress due to its ability to mediate tumour regression in patients with malignant hematologic disorders (4). The CAR molecule features a complex structure with an extracellular domain for antigen recognition linked to an intracellular signaling domain through a transmembrane region (5). Traditionally, the extracellular part includes a single-chain variable

***Corresponding authors:** Mahmoud Hassani. Shahid Beheshti University of Medical Sciences, Tehran, Iran. Tel: +98-218866649, Email: mahmoud.hassani@yahoo.com; Kowsar Bagherzadeh. Iran University of Medical Sciences, Tehran, Iran. Tel: +98-2164351, Email: bagherzadeh.kw@gmail.com

fragment (scFv) from an antibody, allowing antigen binding independently of MHC presentation. However, limitations associated with scFvs have prompted the search for better alternatives. Nanobodies (VHHs), derived from camelid heavy-chain antibodies, offer a smaller, stable, and effective option for antigen recognition and are increasingly used in CAR designs to replace conventional scFvs (6). Depending on the desired signalling pathway and immune response, various intracellular domains, such as CD28, 4-1BB, and OX40, are selected and incorporated into the CAR structure; with these elements being commonly utilized in current research. The CD3ζ domain is consistently involved in intracellular signalling within CAR-T cells. Also nanobody can specifically recognize tumour-associated antigens (TAA), leading to T cell activation in a manner independent of MHCs (5). The transmembrane domain typically consists of the transmembrane regions from proteins such as CD3, CD8, CD28, or FcεRI, and it functions to transmit the activation signal from the scFv into the cell. The intracellular signalling region is composed of domains such as CD134 (OX40), CD28, or CD137 (4-1BB), along with the CD3ζ domain, which contains the immune-receptor tyrosine-based activation motif (ITAM) (7–9). ITAM plays a critical role in the signal transduction process that activates T cells. The identification of suitable antigens for CAR design is the first crucial step in utilizing this technology. The target antigen should be stably expressed on the extracellular membrane and should be specific to cancer cells, avoiding cross-reactivity with healthy cells (10).

Design and development of safe and efficient therapies to fight resistance cancer have become a major concern in the field of cancer immunotherapy. Meanwhile, computational structural biology plays a key role in providing information on the various aspects of biomolecules, small/macro molecules, and their interactions. In this context, the investigation and development of various CAR T-cell models for cancer treatment have special importance. Thus, the aim of our computational study is to compute the impact of adding a structure to target antigen.

Several antigens specific to prostate cancer cells including PSA, PSMA, TARP, and P8 (TRP), have been studied. PSA and PAP, despite their association with prostate tissue, also appear in other organs, limiting their suitability as CAR targets (11). PSMA, a membrane glycoprotein uniquely expressed in prostate cells, has been widely investigated, particularly in imaging and immunotherapy (12). Given the challenges in targeting solid tumors with T cells, NK cells have emerged as a promising alternative due to their ability to infiltrate tissues and promote immune memory (13). CAR-NK cell therapy, facilitated primarily through viral transduction for efficient gene delivery, offers a new strategy for treating solid malignancies like prostate cancer (14, 15).

This study aims to compare the second and third generations of CAR constructs, both with a common extracellular domain targeting the PSMA antigen. The third generation includes an intracellular domain with OX40, while the second generation does not. In this report a third generation CAR construct was designed and developed based on an anti-PSMA nanobody (NBPIII-CAR). The CAR construct was functionally characterized in the NK92 cells after co-culturing with the prostate cancer cells compare second generation CAR (NBPII-CAR) *in vitro*. The two nanobody-based CARs were efficiently expressed on the transduced NK92 cells and could specifically activate the NK92 cells after recognizing PSMA on the prostate cancer cells.

Materials and Methods

Homology modelling and structure evaluation of the modelled target nanobody structures

To determining cell surface expression of CAR on effector cells two tags (c-myc and Flag tags) candidate in CAR context. for this reason, the 3D structures of the all constructs (nanobody(NB), nanobody+hinge(NB-hinge), nanobody+flag+hinge(NB-flag-hinge) and nanobody+c-myc+hinge(NB-cmyc-hinge)) were homology modelled using the I-TASSER webserver (16). The structure quality of the modeled structures was assessed using Ramachandran plot, ProSA (17) and MolProbility (18) webservers. Ramachandran plots were generated via the PROCHECK webserver (19) (Supplementary Information, Tables S1, S2, Figures S1 and S2).

Molecular dynamic simulations

The conformational stability and structural changes of the modeled templates were analysed using molecular dynamic simulations (MDs) performed with GROMACS 2022.6 and the AMBER force field (amber99sb-ildn) (20). The models were solvated in a dodecahedral box filled with TIP3P water molecules with the minimum distance of 1.2 nm between the protein surface and the box walls. The system net charge was neutralized by replacing water molecules with appropriate sodium and chloride counter ions. Electrostatic interactions were computed using the particle mesh Ewald (PME) method, with a van der Waals cut-off of 1.4 nm and periodic boundary conditions applied in all directions. Covalent bonds involving hydrogen were constrained using the LINCS algorithm, which fixes selected bond lengths during integration, reducing high-frequency bond vibrations and improving numerical stability. The system underwent energy minimization using the steepest descent algorithm with a tolerance of 1000 kJ/mol/nm (21, 22).

After convergence, the system was equilibrated using NVT ensemble MD simulations for 100 ps. Subsequent MD simulations were performed using the NPT ensemble under periodic boundary conditions. The Berendsen barostat and thermostat were employed to maintain constant pressure (1 bar) and temperature (300 K) with coupling times of $\tau p = 0.5$ ps and $\tau T = 0.1$ ps, respectively. The production MD simulations were extended to 100 ns under constant pressure and temperature conditions (21, 22). Further analyses were performed using trajectory coordinate files, including root mean square deviation (RMSD), root mean square fluctuation (RMSF), radius of gyration (Rg), solvent-accessible surface area (SASA), hydrogen bond analysis, and secondary structure analysis using the Database of Secondary Structure Assignments (DSSP) (Supplementary Information, Figures S3).

Molecular docking simulations

The binding affinity of the target patterns for PSMA was estimated using the Maestro Molecular Modeling platform (version 13.5) by Schrödinger, LLC (12). The crystallographic structures of PSMA were obtained from the Protein Data Bank (PDB ID: 1Z8L) (http://www.rcsb.org). Initial structures were prepared using the Protein Preparation Wizard module (Schrödinger Release 2020-3: Protein Preparation Wizard; Epik, S., LLC, New York, NY, USA (2020).). This preparation involved the removal of

water molecules, ions, and crystallographic compounds. A series of procedures were then performed, including; hydrogen atoms addition, structure corrections (updating and filling the missing side chains residues for PSMA), hydrogen bonds optimization, atomic clashes omission, formal charge addition and optimization of the hetero groups were performed at neutral pH. Finally, the structures were minimized using optimized potential for liquid simulations (OPLS3) force field.

The interactions and binding energies between the modeled nanobodies and PSMA were calculated using the PIPER wizard of Schrödinger (23, 24). PIPER employs the Fast Fourier Transform (FFT) correlation method, allowing the evaluation of a vast number of conformations. This method is specifically optimized for antibody-antigen pairs, enhancing the accuracy of the results. The docking procedure involved assessing up to 70,000 distinct poses of the nanobody-antigen complex, with no masking applied to non-CDR regions. The top-ranked poses were selected based on their binding energies. Nanobody-antigen interaction analyses were subsequently performed using the Protein Interaction Analysis wizard.

Graphical representation software

The MDs results were analyzed using the VMD 1.9.3 software (25) and visualized using PyMol (*The PyMOL Molecular Graphics System, Version 1.2r3pre*, Schrödinger, LLC). The graphs were all represented with the application of Microsoft Office Excel 2023.

Cell lines

The NK92 cell line was kindly provided by PersisGen Par Biopharma Accelerator, while the human prostate cancer cell lines (LNCaP and PC3) were sourced from the Pasteur Institute of Iran (Tehran, Iran). PC3 cells were cultured in DMEM (Biosera, France), LNCaP cells in RPMI 1640 medium (Biosera), and NK92 cells in α-mem medium enriched 100 IU/ml rhIL2, 100 nanograms per millilite of IL-15 (R&D Systems) and 10% inactivated horse serum (Sigma-Aldrich, USA), all media were further enriched with 10% heat-inactivated fetal bovine serum (Biosera), 100 IU/ml penicillin (Sigma-Aldrich, USA), and 100 µg/ml streptomycin (Sigma-Aldrich). The cell lines were grown at 37 °C with 95% humidity and 5% CO_2

NBPII AND NBPIII-CAR constructs

The CAR constructs used in this study are illustrated schematically in Figure 1. A single-domain antibody fragment (nanobody) targeting PSMA (NBP), generously provided by Dr. W.M. van Weerden, was utilized for target recognition (PSMA) in the CAR construct (6). The intracellular activation domains of human CD28 and the activating components of CD3ζ were linked to the transmembrane domain of CD28, and this complex was connected to the nanobody via a spacer (Flag hinge CH2-CH3) to ensure flexibility in the extracellular region. This construct represents a second-generation CAR, referred to as NBPII-CAR (Figure 1). The NBPIII-CAR structure was designed similarly to the NBPII, with the only difference being the addition of the OX40 intracellular domain after the CD28 domain. Both generations of CARs were synthesized by Biomatik (Cambridge, Canada) and subcloned into the mammalian expression vector PCDH (Invitrogen, CA, USA), designated as pNBPII-CAR and pNBPIII-CAR. Following verification by colony PCR, restriction enzyme

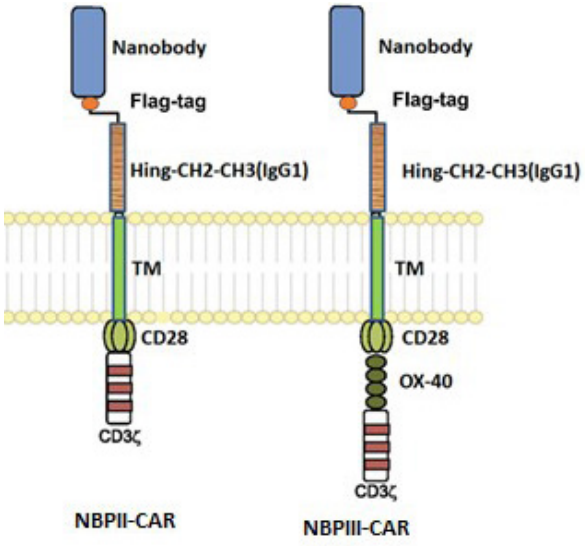

Figure 1. Schematic design of both generations of Chimeric Antigen Receptor (CAR) structures is shown in this picture, according to which the extracellular part of both structures is the same and includes an antigen-recognizing nanobody and a membrane binder of IgG1

The intracellular part links to the transmembrane part of Cluster of differentiation 28 (CD28) and next to it is the intracellular part of cluster of differentiation 28 (CD28), and then in the second generation, cluster of differentiation 28 (CD28) connects to cluster of differentiation Zeta (CD3ζ), and in the third generation, after cluster of differentiation 28 (CD28), the cluster of differentiation 134 (OX40) domain is placed, and then cluster of differentiation Zeta (CD3ζ).

mapping, and sequencing, the plasmid was propagated in *E. coli* (DH5α) (26).

Packaging and transduction of NBPII/III CAR-encoding lentiviral vectors

To generate lentiviral vectors, 8 × 10^6 Lenti-X 293T cells (Clontech Laboratories, USA) were cultured in a 10 cm plate in Dulbecco's Modified Eagle Medium (DMEM) (Gibco, USA) supplemented with 10% FBS, 100 µg/ml streptomycin, and 100 units/ml penicillin. The cells were incubated at 37 °C in a humidified 5% CO_2 chamber for 24 hr prior to transfection. The second-generation lentivirus packaging system, which included psPAX and pMD2.G packaging plasmids, was co-transfected with the pCDH-CAR constructs into the Lenti-X 293T cells using the PEI transfection reagent (Sigma, USA) according to the manufacturer's instructions. The supernatant was collected every 24 hr over a three-day period. The collected supernatants were centrifuged at 50,000 × g for 90 min at 4 °C, followed by filter sterilization and storage at -80 °C for future use (15, 27).

NK92 cells transduction

CAR-encoding lentiviruses at a multiplicity of infection (MOI) of 10, along with polybrene at a final concentration of 8 µg/ml (Sigma, USA), were added to NK92 cells in 6 cm^2 dishes. The cells were centrifuged at 400 × g for 90 min at 32 °C and then incubated for 24 hr. the culture medium being changed every 48 hr. Recombinant human IL-2 (rhIL-2) at a concentration of 100 IU/ml and 100 ng/ml of IL-15 (R&D Systems, UK) was routinely added to the culture medium (28). Ten days after antibiotic pressure, transfected NK92 cells were tested for functionality.

Detecting the cell surface expression of CAR and PSMA

A Flag tag was incorporated into the CAR construct based on computational analysis to facilitate detection of

CAR expression on transduced effector cells. One million transduced and non-transduced cells were incubated with PE-conjugated anti-DYKDDDDK Tag (Flag tag) antibody (BioLegend, Inc.) at 4 °C for 45 min, washed with PBS, resuspended, and analyzed by flow cytometry. To assess PSMA expression on target cells, one million LNCaP and PC3 cells were first washed with PBS, incubated with an anti-human PSMA (FOLH1) antibody at 4 °C for 45 min, washed, and then incubated with a FITC-conjugated anti-mouse IgG secondary antibody (BioLegend, Inc.) at 4 °C for 30 min. After two additional PBS washes, the cells were resuspended and analyzed by flow cytometry to determine PSMA surface expression.

Analysis of cytokine production

Transduced NK92 cells (2×10^4) were co-cultured with LNCaP and PC3 target cells at Effector:Target (E:T) ratios of 1:1, 5:1, and 10:1. After 24 hr, the culture supernatants were collected, and the concentrations of TNFα, IFN-γ, and IL-2 were quantified using a commercial ELISA kit (Karmania Pars Gene Company, Iran) according to the manufacturer's instructions.

Cytotoxicity assays

Transduced and non-transduced NK-92 cells (2×) were co-cultured with target cells (LNCaP and PC-3) at three different Effector:Target (E:T) ratios of 1:1, 5:1, and 10:1. After 4 hr, cytotoxicity was evaluated using the LDH Cytotoxicity Assay Kit (DoGenBio, DG-LDH500) according to the manufacturer's instructions. Briefly, 10 µl of the supernatant from both control and test groups was incubated with 100 µl of the LDH reaction mixture in 96-well plates. After a brief incubation, absorbance was measured at 450 nm The cytotoxicity percentage was calculated using the following standardized formula where 'Experimental release' is the absorbance of the co-culture (effector + target cells), 'Spontaneous release' is the LDH activity of target cells alone (background release), and 'Maximum release' is the absorbance of target cells treated with lysis buffer (total LDH content). All values were corrected by subtracting the culture medium background absorbance (29, 30).

Statistical analysis

A Student's t test was used to compare two value sets, while we used one-way ANOVA when three groups were involved. Histograms represent mean values ± standard deviations, $P<0.01$, or $P<0.001$ were indicated by *, or ** respectively. Graph Pad Prism 7.0 software was used for all the statistical analyses.

Results

Homology modelling and evaluation

The ProSA plots indicate that the overall structural quality of the modeled nanobodies falls within the range of scores typically observed for native proteins of similar size. The MolProbity scores further assess the resolution of the models in comparison to X-ray crystal structures. Lower values in the ProSA Z-score and MolProbity scores denote higher structural quality (Supplementary Information, Figures S1 and S2). The results demonstrate that the modeled protein structures remained stable following molecular dynamics simulations (MDS) and exhibited reliable quality (Supplementary Information, Table S2).

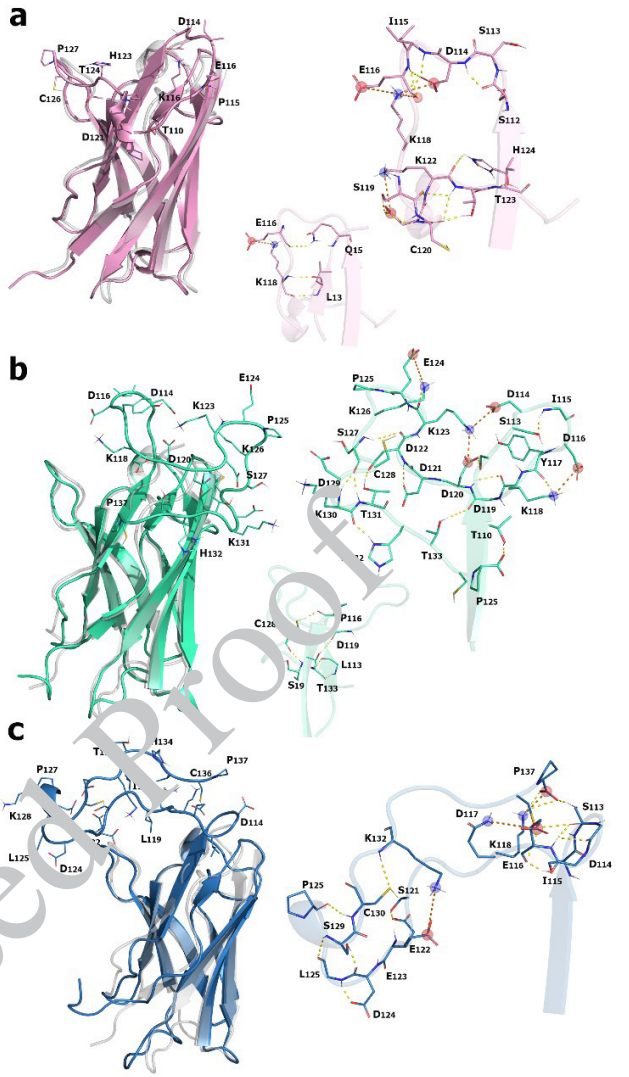

Figure 2. Superimposition of a. Nanobody+hinge (NB/hinge), b. Nanobody+Flag+hinge (NB/Flag/hinge), and c. Nanobody+c-myc+hinge (NB/c-Myc/hinge) over lone Nanobody (NB) (in light gray) and the close view of the hinge, Flag/hinge and c-Myc/hinge sequence structures and the participant residue interactions, respectively.
The hydrogen bonds are represented in yellow dashes and the salt bridges are represented in orange dashes.

Molecular dynamic simulations of the target nanobodies

The behavior of the modelled structures was thoroughly monitored during MDs (Figure 2). The root mean square deviation (RMSD) and root mean square fluctuation (RMSF) plots for the target nanobodies are presented in *Supplementary Information, Figure S3*. Accordingly, the homology modelled structures of the designed nanobodies were submitted to 100 ns of MDs and the final trajectories were analysed.

The RMSD and per-residue RMSF of the nanobodies structures were computed (*Supplementary Information, Figures S3a and b*) that show the least structural deviation and fluctuation for NB and NB/Flag/hing. While the RMSD plot of NB is equilibrated during the simulation time, the NB/Flag/hing, NB/c-Myc/hinge plots attain equilibration state after 40 ns and 80 ns of MDs, and the NB/hinge structure does not reach the steady state in the monitored simulations time. Addition of Flag/hinge sequence to the NB results in a network of hydrophobic interactions not

only between the added residues, but with the NB main body which is further supported by salt bridges and electrostatic interactions (Figures 2a, b, and c). Also, addition of hinge to the NB induce drastic conformation changes in the NB's structure that is evident from the RMSD and RMSF plots. This observation is further supported by protein gyration and SASA plots (Supplementary Information, Figures S3c and d).

Although absent of large SASA fluctuations in the plots of the studied NBs indicate relatively high inter-peptide stability, the plots show that the structure with added Flag/hinge behave similarly to that of lone NB. A similar trend is also observed in the radius of gyration (Rg) plots throughout the MD simulations. the considerable fluctuations in the NB/hinge Rg plot suggest significant changes in the nanobody structure are affecting the compactness of the protein.

As it is evident, the hinge region sequence length and participant residues affect the conformation of the initial NB that consequently results in higher values of RMSF, RMSD, SASA, and radius of gyrations for the derived structures, among which, NB/Flag/hinge, shows the least fluctuations and closest behavior to the lone NB (Supplementary Information, Figures S3c and d). The observation can be attributed to the formation of a network of hydrogen bonds and salt bridges in between the Flag/hinge participant residues and their interactions with the NB participant residues (S19, T10, and L113) that limits the residue fluctuations in the added sequence as well as the whole NB (Figure 2b). This evidence is further supported by the Secondary Structure Assignments (Supplementary Information, Figures S3e) that shows an increase in the number of residues in the NB structure after addition of the Flag/hinge. Similar network of interactions is also observed between the hinge participant residues with each other and with the main NB in NB/hinge structure (Figure 2b), but the interactions are inducing drastic conformational changes in the NBs structure that are quite evident from analysis (Supplementary Information, Figures S3). On the other hand, the c-Myc/hinge participant residues do not establish interactions with the NB construct (Figure 2c).

Molecular docking simulations of the target NBs over PSMA

The equilibrated structures were then submitted for the molecular docking studies over PSMA employing PIPER wizard of Schrödinger for antibody-antigen docking studies (Figure 3). The top rank complexes obtained from docking studies of nanobodies with PSMA were thoroughly studied and the interaction sites and mode of interactions were analyzed. According to the obtained results (*Supplementary Information*, *Table S3*), NB/Flag/hinge shows the highest affinity for PSMA with PIPER pose energy of -225.179 and PIPER pose score of -345.131 in the cluster with the most participant docking poses and the least affinity form PSMA is observed for NB-hinge with PIPER pose energy of -176.623 and PIPER pose score of -161.509.

Cell surface expression analysis

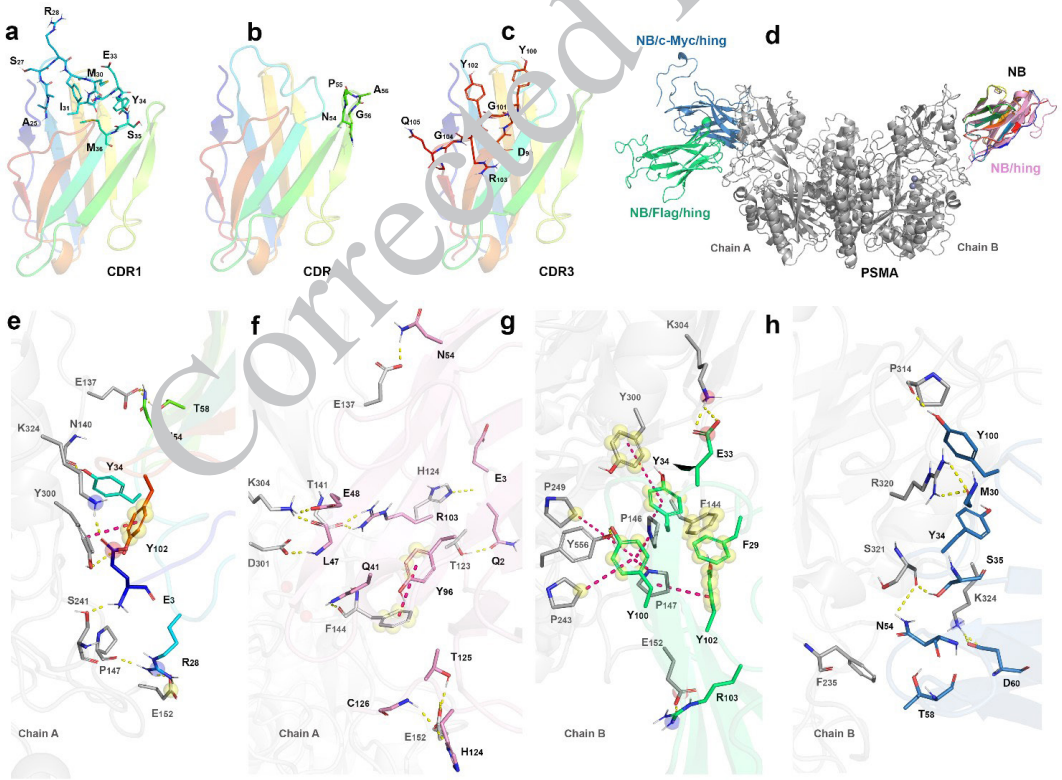

Figure 3. NB structure with an emphasize on:
a. Complementarity-determining region 1 (CDR1) region, b. Complementarity-determining region 2 (CDR2) region, and c. Complementarity-determining region 3 (CDR3) region, as well as d. Overall docking pose of the studied NBs (lone nanobody (NB) in rainbow, nanobody (NB/hinge) in pink, nanobody+Flag+hinge (NB/Flag/hinge) in green and nanobody+c-Myc+hinge (NB/ c-Myc/hinge) in blue) over prostate specific membrane antigen (PSMA) along with the close view of the interacting residues for e. Lone nanobody (NB), f. Nanobody (NB/hinge), g. Nanobody+Flag+hinge (NB/Flag/hinge), and h. Nanobody+c-Myc+hinge (NB/ c-Myc/hinge) in complex with prostate specific membrane antigen (PSMA)
The hydrogen bonds are represented in yellow dashes, the salt bridges are represented in orange dashes and the electrostatic interactions are represented in magenta dashes.

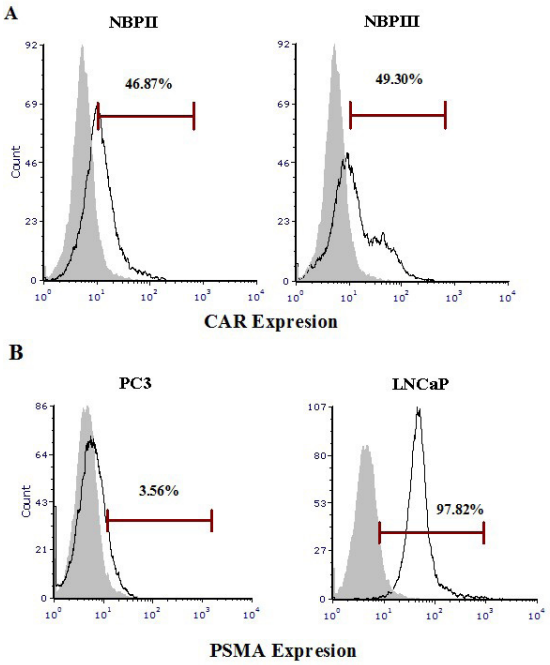

Figure 4. Cell surface expression of chimeric antigen receptor (CAR) and prostate specific membrane antigen (PSMA)
A: Flow cytometry analysis of surface expression of car structure in transduced cells whit phycorythrin (PE) labeled antibody against nanobody Transduced cells with third-generation construct (NBPIII) show about 49% phycorythrin (PE) labeled antibody binding and transduced cells with second-generation construct (NBPII) show about 47% phycorythrin (PE) labeled antibody binding the black histogram shows transduced Natural Killer 92 cell line (NK92) and the grey histogram represents control Natural Killer 92 cell line (NK92) cell not transduced, B: Examining the surface expression of prostate specific membrane antigen (PSMA) antigen on the surface of target cells using fluorescein Isothiocyanate (FITC) labeled antibody against prostate specific membrane antigen (PSMA) expression in lymph node carcinoma of the prostate (LNCaP) cells is about 98%. and prostate specific membrane antigen (PSMA) expression in prostate cancer-3 (PC3) cells is about 3.5%. The black histogram shows cells with fluorescein isothiocyanate (FITC) antibody and the grey histogram represents the control cell.

Post-transduction, GFP expression was first verified, and the transduced cells were visualized using fluorescence microscopy. To assess the surface expression of the CAR construct, flow cytometry was performed using PE anti-DYKDDDDK Tag Antibody (BioLegend, Inc.). Representative results showed that 47% of the transduced NK cells expressed the NPBII CAR, and 49% expressed the NBPIII CAR (Figure 4A). The PSMA expression on the target cells (LNCaP and PC3) was determined by flow cytometry using a PE-conjugated anti-PSMA antibody. On the basis of the expression of PSMA, as shown in Figure 4B, LNCaP cell was considered a positive and DU-145 cell a negative target cell.

Cell activation and cytotoxicity of CAR NK cells upon co-culturing with the target cells

CAR-induced cytokine secretion

In this study, we have utilized the levels of INFγ, TNFα, and IL2 secretion as markers of NK cell activation. After the co-culture of NK cells, transduced with both generations of CAR as effector cells, with LNCaP target cells as PSMA positive and PC3 cells as PSMA negative, we evaluated the expression of these markers. It is found that due to the increased expression of these markers, NK cells with the third generation have a significantly better performance against the target cell than the second generation. According to Figure 5 and the examination and comparison of the expression of the markers, it is observed that in the NBPIII CAR NK-92 cells with the target cell, compared to the NBPII CAR NK-92 cells, the expression of TNFα is 1300 pg/ml in the NBPIII and 990 pg/ml in the NBPII. The expression of INFγ is 730 pg/ml in the NBPIII and 550 pg/ml in the NBPII, and the expression of IL2 is 850 pg/ml in the NBPIII and 490 pg/ml in the NBPII. Our results demonstrated that NBPII/III-CAR NK cells, in comparison to the parental

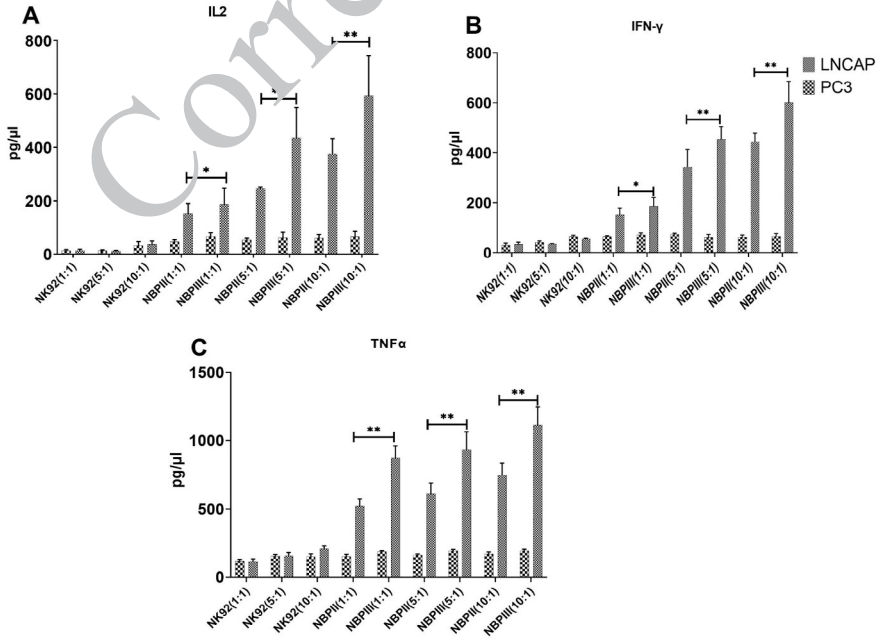

Figure 5. Cytokine production by CAR-NK92 cells co-cultured with prostate cancer cell lines
(A) Interleukin-2 (IL-2), (B) Interferon gamma (IFN-γ), and (C) Tumor necrosis factor alpha (TNFα) levels in the supernatant were measured by enzyme linked immunosorbent assay (ELISA) after 24 hr of co-culture between CAR-transduced NK92 cells (NBPII and NBPIII) and lymph node carcinoma of the Prostate (LNCaP) (prostate specific membrane antigen (PSMA)$^+$) or prostate cancer-3 (PC3) (prostate specific membrane antigen (PSMA)$^-$) cells at effector-to-target (E:T) ratios of 1:1, 5:1, and 10:1. NBPIII CAR-NK92 cells exhibited significantly higher cytokine production compared to NBPII CAR-NK92 cells, particularly in response to prostate specific membrane antigen (PSMA)$^+$ lymph node carcinoma of the prostate (LNCaP) targets. Values are shown as mean ± standard deviation (SD). Statistical significance: *P<0.01, **P<0.001.

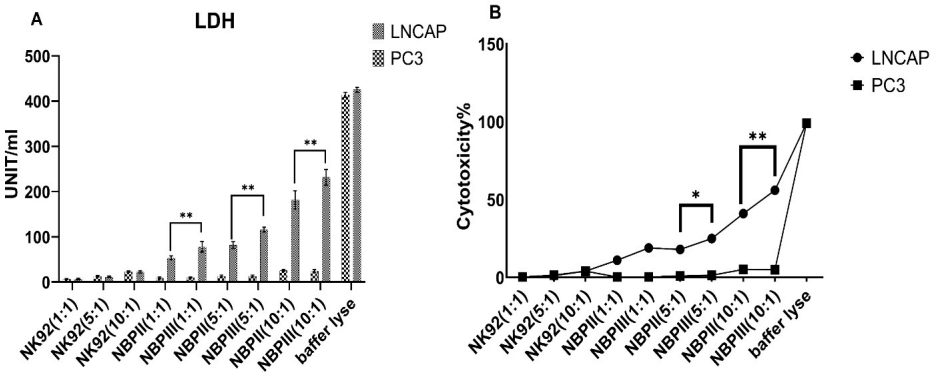

Figure 6. Cytotoxic activity of CAR-NK92 cells against prostate cancer cell lines
(A) Lactate dehydrogenase (LDH) release assay showing the cytotoxicity of second-generation (NBPII) and third-generation (NBPIII) CAR-NK92 cells against lymph node carcinoma of the prostate (LNCaP) (prostate specific membrane antigen (PSMA)$^{+}$) and prostate cancer-3 (PC3) (prostate specific membrane antigen (PSMA)$^{-}$) target cells at E:T ratios of 1:1, 5:1, and 10:1. (B) Cytotoxicity percentage calculated from LDH release data confirms higher killing activity by NBPIII-CAR cells, particularly at the 10:1 ratio. Lymph node carcinoma of the prostate (LNCaP) cells exhibited significantly greater sensitivity than prostate cancer-3 (PC3) cells, consistent with their prostate specific membrane antigen (PSMA) expression status. Data are presented as mean ± standard deviation (SD). Statistical significance is indicated as *P<0.01 and **P<0.001.

NK92 Cell group, had a statistically significant higher level of cytokine secretion (42 ± 1.6 pg/ml TNFα and 61 IL2 and 4.9 pg/ml of INFγ). Additionally, the data from this study indicate that the cytotoxicity rate is significantly higher in the NBPIII CAR structure compared to the NBPII (in 5:1 and 10:1), as illustrated in Figure 6.

LDH assay for cytotoxicity assessment

The cytotoxic activity of engineered NK92 cells was analyzed using the LDH release assay. As shown in Figure 6, both CAR-modified NK92 cells were able to lyse LNCaP, but not PC3 cells (in all three ratios). These data show that NK92 cells do not have cytotoxic properties against prostate cancer cells (LNCaP and PC3), and their cytotoxicity can be shown through modifications using the CAR structure. Additionally, the data from this study indicate that the cytotoxicity rate is significantly higher in the NBPIII CAR structure compared to the NBPII (in 5:1 and 10:1), as illustrated in Figure 6.

Discussion

Our previous study showed that the second-generation PSMA-CAR T cells could be activated by target cells (PSMA-positive cells) and kill them (6,26). Considering the advantages that NK cells have over T cells in solid tumors, one of the objectives of this study is replacing T cells with NK cells and the other one developing a third-generation CAR NK-92 cells with OX-40 to evaluate the effect of its addition on the activation of PSMA-CAR NK-92 cells. Following an *in silico* study for selecting an optimize tag for CAR expression, First, NK92 cells were transduced with lentiviral particles and CAR expression on NK-92 cells confirmed after, their activity was assessed *in vitro* against LNcAP and PC3 cell lines. Our data showed that activation by NBPIII CAR NK-92 cells resulted in more efficient expression of IL2, TNFα and INFγ production, as compared with NBPII CAR NK-92 cells. Additionally, LDH assay showed cytolytic activity was significantly higher in case of NBPIII CAR NK-92 cells.

Design and development of safe and efficient therapies to fight resistance cancer have become a major concern in the field of cancer immunotherapy. Meanwhile, computational structural biology plays a key role in providing information on the various aspects of biomolecules, small/macro molecules, and their interactions. Researchers are actively investigating and developing various models of CAR T-cell therapy to fight cancer. The aim of the computational study was to compute the impact of adding an optimize tag on the initial CAR structure and its interactions with the target antigen, PSMA.

These RMSD and RMSF plots of the studied structures reveal that the nanobody and NB/Flag/hinge exhibit the least structural deviations and per-residue fluctuations, indicating higher stability compared to NB/hinge and NB/c-Myc/hinge (Supplementary Information, Figure S3). The radius of gyration (Rg) plots show that the nanobody and NB/Flag/hinge achieved compact structures earlier in the simulation and maintained relaxation for the remainder of the simulation time. Additionally, the lower solvent accessible surface area (SASA) values for these two constructs suggest relatively higher inter-peptide stability. Secondary structure analysis was employed to further evaluate the structures of the target nanobodies. The results reveal significant refolding in the percentage of residues contributing to the overall structure of NB/Flag/hinge compared to NB, NB/hinge, and NB/c-Myc/hinge.

Further, according to the docking studies, NB/Flag hinge reveals the highest affinity for PSMA with PIPER pose energy of -225.179 and PIPER pose score of -335.131 (Supplementary Information, Table S3). The NB/Flag hinge interacts the apical region of chain A through CDR1 and CDR3 regions by establishment of several π-stack, π-alkyl, hydrogen bonds and salt bridges (Figure 2). Establishment of a network of electrostatic interactions between the aromatic residues in the binding interface, including F29, Y34, Y100, and Y102 from the NB and residues F 144, P146, P147, P243, P249, Y300, and Y556 from PSMA results in a significantly higher affinity of the NB/Flag hinge in comparison to those of others. The electrostatic network is further strengthened through conventional hydrogen bonds and salt bridge formation between R103 in CDR3 and E33 in CDR1 regions with residues E152 and K304 in PSMA (Figure 2c, Supplementary Information, Table S4). Accordingly, the NB/Flag/hinge interacts PSMA through electrostatic complementarity while the rest of the studied NBs establish hydrophobic complementarity with the antigen while the shape/surface complementarity is almost identical.

Chimeric Antigen Receptor (CAR) technology has been widely employed to direct autologous engineered T cells for the treatment of hematologic malignancies (1). The most notable success in treating acute lymphoblastic leukaemia (ALL) has been with CD19-CAR, achieving a 90% remission rate in patients resistant to other treatments (1, 31). However, the use of autologous T cells presents certain limitations. The production of engineered autologous T cells is challenging and often insufficient for widespread clinical application (13). Moreover, the process of generating patient-specific CAR-T cells typically requires several weeks, which can be problematic for patients with rapidly progressing disease (4). Additionally, obtaining a sufficient quantity of T cells from patients who have undergone multiple rounds of chemotherapy is challenging. Developing an off-the-shelf allogeneic product could help address this issue (19). However, the use of allogeneic T cells increases the risk of graft-versus-host disease (GVHD) due to interactions between the T cell receptor (TCR) of the recipient's T cells and the donor cells' HLA molecules (20, 21). Given that natural killer (NK) cells are potent cytotoxic cells that can non-specifically identify targets and do not cause GVHD, they represent a promising alternative for developing allogeneic products in CAR technology (6). Due to the inherent cytotoxicity of NK cells and their unique ability to target and identify cancer cells that lack specific antigens a limitation of CAR-T cell therapy that can lead to disease relapse NK cells offer a potential solution to this issue (18). These intrinsic properties of NK cells make them particularly appealing for use in CAR technology within cancer immunotherapy (6). Identifying and targeting specific antigens for engineered effector cells is a crucial step in CAR technology-based immunotherapy. In this study, the performance of both generations in NK-92 cells has been demonstrated effectively. The secreted cytokine profile indicates that both generations are activated upon encounter with PSMA-positive cells, leading to cytokine secretion.

The utilization of nanobodies as functional molecules is experiencing significant growth and is increasingly being adopted in various studies. They have been recognized as a viable alternative to single-chain variable fragments (scFvs). Notably, Carvykti® (ciltacabtagene autoleucel) (anti BCMA CAR based on nanobody) has recently received approval from the U.S. Food and Drug Administration for the treatment of multiple myeloma. In this study, based on the numerous advantages associated with nanobodies (including their monomeric construction, very low immunogenicity, high specificity, and most importantly, their ability to target hidden or buried epitopes), VHH was employed as a suitable alternative to scFv within the CAR structure (32, 33).

Incorporating the OX40 co-stimulatory domain into CAR T cell constructs has demonstrated several functional advantages. Finny *et al.*, demonstrated that OX40 signaling contributes to enhanced T cell persistence and mitigates exhaustion, which are critical for maintaining long-term anti-tumor activity (34). Furthermore, Moreno-Cortes *et al.*, report that incorporating the OX40 co-stimulatory domain into CAR T cells, alongside ICOS, enhances their cytotoxic activity and promotes a central memory T-cell phenotype, leading to improved persistence and antitumor efficacy both *in vitro* and *in vivo* (34). In addition, CAR T cells equipped with OX40 domains have shown greater cytokine release and cytotoxicity *in vitro*, indicating more robust effector function against tumor targets (27). Given this background, we anticipated that CAR-modified NK-92 cells contain OX-40 co-stimulatory (as a third-generation CAR) would be superior to second-generation. Our data shows the addition of OX-40 signalling domain promotes NK cell activation, leading to increased cytokine production and cytotoxicity against tumor cells.

The Prostate-Specific Membrane Antigen (PSMA) is a non-secreted membrane glycoprotein with carboxypeptidase and folate hydrolase activity, characterized by a large extracellular domain (35). In investigating the PSMA ligand and its receptors using radiolabels, it was found that after the ligand binds to the PSMA receptor, it enters the cell and remains active in cancer cells for a longer duration than in healthy cells. Due to its large extracellular domain, PSMA is an ideal target for prostate cancer treatment through immunotherapy (2, 36).

Conclusion

In this study, a third-generation nanobody-based CAR-modified NK-92 cell line was designed, employing an optimized tag to identify PSMA on prostate cancer cells, leading to the activation of these engineered cells and the selective destruction of prostate cancer cell lines. These findings strongly indicate the potential of utilizing CAR-modified NK-92 cells with nanobodies for targeted immunotherapy. The findings highlight the potential of nanobody-based CAR-NK92 cells as a promising approach for targeted immunotherapy and support their further development toward clinical application in prostate cancer treatment.

Acknowledgment

The results presented in this paper were part of a student thesis.

Ethical Approval

This study does not involve human participants, animals, or any biological samples directly. The computational work, including molecular modeling, docking, and machine learning analyses, was conducted using publicly available datasets and tools. For compliance, this study was reviewed and approved by the Medical Nanotechnology and Tissue Engineering Research Center, Shahid Beheshti University of Medical Sciences, Tehran, Iran (approval code NO. IR.SBMU.RETECH.REC.1400.284).

Funding

This work was supported by Medical Nanotechnology and Tissue Engineering Research Center (Grant number 27705) and Iran National Science Foundation (INSF) (Grant number 4002248).

Authors' Contributions

M GGh, A KV, A R, F HT, Z S, and N T performed the majority of the experimental and computational work. M A and M S provided expert supervision. WMVW supplied the anti-PSMA nanobody. M B contributed to resource provision. M H and K B, as corresponding authors, played key roles in study design, project supervision, and funding acquisition.

Conflicts of Interest

The authors declare no competing interests.

Declaration

We acknowledge the use of Deep Seek for language editing and for generating suggestions to improve the clarity and readability of the manuscript.

References

1. Fay EK, Graff JN. Immunotherapy in prostate cancer. Cancers (Basel) 2020;12:1–17.
2. Wang F, Li Z, Feng X, Yang D, Lin M. Advances in PSMA-targeted therapy for prostate cancer. Prostate Cancer Prostatic Dis 2022;25:11–26.
3. Maude SL, Laetsch TW, Buechner J, Rives S, Boyer M, Bittencourt H, *et al.* Tisagenlecleucel in children and young adults with B-cell lymphoblastic leukemia. N Engl J Med 2018;378:439–448.
4. Hartmann J, Schussler-Lenz M, Bondanza A, Buchholz CJ. Clinical development of CAR T cells-challenges and opportunities in translating innovative treatment concepts. EMBO Mol Med 2017;9:1183–1197.
5. Gong Y, Klein Wolterink RGJ, Wang J, Bos GMJ, Germeraad WT V. Chimeric antigen receptor natural killer (CAR-NK) cell design and engineering for cancer therapy. J Hematol Oncol 2021;14:73.
6. Hassani M, Hajari Taheri F, Sharifzadeh Z, Arashkia A, Hadjati J, van Weerden WM, *et al.* Construction of a chimeric antigen receptor bearing a nanobody against prostate a specific membrane antigen in prostate cancer. J Cell Biochem 2019;120:10787–10795.
7. Guercio M, Orlando D, Di Cecca S, Sinibaldi M, Boffa I, Caruso S, *et al.* CD28. OX40 co-stimulatory combination is associated with long in vivo persistence and high activity of CAR. CD30 T cells. Haematologica 2020;106:987.
8. Chikileva IO, Bruter A V, Persiyantseva NA, Zamkova MA, Vlasenko RY, Dolzhikova YI, *et al.* Anti-cancer potential of transiently transfected HER2-specific human mixed CAR-T and NK cell populations in experimental models: Initial studies on Fucosylated chondroitin Sulfate usage for safer treatment. Biomedicines 2023;11:2563.
9. Moreno-Cortes E, Franco-Fuquen P, Garcia-Robledo JE, Forero J, Booth N, Castro JE. ICOS and OX40 tandem co-stimulation enhances CAR T-cell cytotoxicity and promotes T-cell persistence phenotype. Front Oncol 2023;13:1200914.
10. Montagner IM, Penna A, Fracasso G, Carpanese D, Dalla Pietà A, Barbieri V, *et al.* Anti-PSMA CAR-engineered NK-92 Cells: An off-the-shelf cell therapy for prostate cancer. Cells 2020;9:1382.
11. Zhang C, Oberoi P, Oelsner S, Waldmann A, Lindner A, Tonn T, *et al.* Chimeric antigen receptor-engineered NK-92 cells: an off-the-shelf cellular therapeutic for targeted elimination of cancer cells and induction of protective antitumor immunity. Front Immunol 2017;18:533.
12. Maurer T, Eiber M, Schwaiger M, Gschwend JE. Current use of PSMA–PET in prostate cancer management. Nat Rev Urol 2016;13:226–235.
13. Vivier E, Rebuffet L, Narni-Mancinelli E, Cornen S, Igarashi RY, Fantin VR. Natural killer cell therapies. Nature 2024;626:727–736.
14. Rahimmanesh I, Totonchi M, Khanahmad H. The challenging nature of primary T lymphocytes for transfection: effect of protamine sulfate on the transfection efficiency of chemical transfection reagents. Res Pharm Sci 2020;15:437–446.
15. Hajari Taheri F, Hassani M, Sharifzadeh Z, Behdani M, Arashkia A, Abolhassani M. T cell engineered with a novel nanobody-based chimeric antigen receptor against VEGFR2 as a candidate for tumor immunotherapy. IUBMB Life 2019;71:1259–1267.
16. Zhou X, Zheng W, Li Y, Pearce R, Zhang C, Bell EW, *et al.* I-TASSER-MTD: A deep-learning-based platform for multi-domain protein structure and function prediction. Nat Protoc 2022;17:2326–2353.
17. Wiederstein M, Sippl MJ. ProSA-web: interactive web service for the recognition of errors in three-dimensional structures of proteins. Nucleic Acids Res 2007;35:W407–W410.
18. Williams CJ, Headd JJ, Moriarty NW, Prisant MG, Videau LL, Deis LN, *et al.* MolProbity: More and better reference data for improved all-atom structure validation. Protein Sci 2018;27:293–315.
19. Laskowski RA, MacArthur MW, Thornton JM. Other validation tools. Int Tables Crystallogr 2012;F:684–687.
20. Clatot J, Currin CB, Liang Q, Pipatpolkai T, Massey SL, Helbig I, *et al.* A structurally precise mechanism links an epilepsy-associated KCNC2 potassium channel mutation to interneuron dysfunction. Proc Natl Acad Sci 2024;121:e2307776121.
21. Rahmati S, Bagherzadeh K, Arab SS, Torkashvand F, Amanlou M, Vaziri B. Computational designing of the ligands of Protein L affinity chromatography based on molecular docking and molecular dynamics simulations. J Biomol Struct Dyn 2024;42:12282–12292.
22. Rahmati S, Torkashvand F, Amanlou M, Bagherzadeh K, Fard Esfahani P, Aghamirza Moghim Aliabadi H, *et al.* Computational engineering of protein L to achieve an optimal affinity chromatography resin for purification of antibody fragments. Anal Chem 2021;93:15253–15261.
23. Chuang G-Y, Kozakov D, Brenke R, Comeau SR, Vajda S. DARS (Decoys as the reference state) potentials for protein-protein docking. Biophys J 2008;95:4217–4227.
24. Kozakov D, Brenke R, Comeau SR, Vajda S. PIPER: An FFT-based protein docking program with pairwise potentials. Proteins Struct Funct Bioinforma 2006;65:392–406.
25. Humphrey W, Dalke A, Schulten K. VMD: Visual molecular dynamics. J Mol Graph 1996;14:33–38.
26. Hassani M, Hajari Taheri F, Sharifzadeh Z, Arashkia A, Hadjati J, van Weerden WM, *et al.* Engineered jurkat cells for targeting prostate-specific membrane antigen on prostate cancer cells by nanobody-based chimeric antigen receptor. Iran Biomed J 2020;24:81–88.
27. Taheri FH, Hassani M, Sharifzadeh Z, Behdani M, Abdoli S, Sayadi M, *et al.* Tuning spacer length improves the functionality of the nanobody-based VEGFR2 CAR T cell. BMC Biotechnol 2024;24:1.
28. Suck G, Odendahl M, Nowakowska P, Seidl C, Wels WS, Klingemann HG, *et al.* NK-92: An "off-the-shelf therapeutic" for adoptive natural killer cell-based cancer immunotherapy. Cancer Immunol Immunother 2016;65:485–492.
29. Yang L, Shen M, Xu LJ, Yang X, Tsai Y, Keng PC, *et al.* Enhancing NK cell-mediated cytotoxicity to cisplatin-resistant lung cancer cells via MEK/Erk signaling inhibition. Sci Rep 2017;7:7958.
30. Chava S, Bugide S, Gupta R, Wajapeyee N. Measurement of natural killer cell-mediated cytotoxicity and migration in the context of hepatic tumor cells. J Vis Exp 2020;22:3791.
31. Nevedomskaya E, Baumgart SJ, Haendler B. Recent advances in prostate cancer treatment and drug discovery. Int J Mol Sci 2018;19:1359.
32. Jin B, Odongo S, Radwanska M, Magez S. Nanobodies®: A review of generation, diagnostics and therapeutics. Int J Mol Sci 2023;24:5994.
33. Bannas P, Hambach J, Koch-Nolte F. Nanobodies and nanobody-based human heavy chain antibodies as antitumor therapeutics. Front Immunol 2017;8:1603.
34. Finney HM, Akbar AN, Lawson ADG. Activation of resting human primary T cells with chimeric receptors: costimulation from CD28, inducible costimulator, CD134, and CD137 in series with signals from the TCRζ chain. J Immunol 2004;172:104–113.
35. Caroli P, Sandler I, Matteucci F, De Giorgi U, Uccelli L, Celli M, *et al.* 68 Ga-PSMA PET/CT in patients with recurrent prostate cancer after radical treatment: Prospective results in 314 patients. Eur J Nucl Med Mol Imaging 2018;45:2035–2044.
36. Vinay DS, Kwon BS. 4-1BB (CD137), an inducible costimulatory receptor, as a specific target for cancer therapy. BMB Rep 2014;47:122.